DIRECT POWER CONTROL OF ACTIVE FILTERS WITH AVERAGED SWITCHING FREQUENCY REGULATION

Su Chen
Department of Electrical and Computer Engineering,
Concordia University, 1455 de Maisonneuve W.,
Montréal, Québec, CANADA H3G 1M8
Email: ches@ece.concordia.ca

Géza Joós
Department of Electrical and Computer Engineering,
McGill University, 3480 University Street,
Montréal, Québec, CANADA H3A 2A7
Email: joos@ece.mcgill.ca

Abstract – **This paper develops a direct power control structure to improve the performance of active filters. The PWM switching functions are defined based on the *instantaneous power terms and the bandwidths of the two* hysteresis comparators are dynamically adjusted to limit the averaged switching frequency. The controller directly uses the instantaneous power as control variables, to replace the current and voltage variables used in multi-loop control systems. It demonstrates that full control of the active filter, including the line current and the dc-bus voltage, can be realized within an integrated control loop. The advantages of the proposed control strategy are verified by simulation and experimental results on a 2 kVA laboratory prototype.**

I. INTRODUCTION

Active filters are commonly used to compensate the harmonics caused by nonlinear loads. Literature [11] shows that most of the active filters use current control method, based on a cascaded multi-loop control structure. The inner current loop compensates harmonics and reactive power, and the outer voltage loop regulates the dc bus capacitor voltage. The current controller either cancels out the line current harmonics or forces the line current to be sinusoidal. Typically, the dynamic response of the inner current loop is fast and that of the outer voltage loop is slow, and the dc-link capacitor must have a sufficient energy storage capability to maintain a stable dc bus voltage during transients. In addition, an appropriate pulse width modulation scheme should be selected to minimize the harmonic injection into the ac systems due to the switching action of the power converters.

A number of new techniques have recently been proposed to improve the control of PWM converters for a number of applications. Issues addressed are the reduction of the number of sensors, alternate modulation schemes and the integration of control and modulation functions. The latter schemes have the advantage of faster transient response and the possibility of controlling simultaneously more than one variable. Among these schemes, the direct torque control (DTC) has been successfully applied in high performance induction motor drives, for both the cage rotor [6][7] and the wound rotor [9] configurations. These methods of control are computationally simple and do not require rotor position sensors. The control schemes for synchronous rectifiers similar to the induction motor DTC, Direct Power Control (DPC) methods, have also been explored [1][2][3]. In these schemes, the instantaneous active and reactive power are directly controlled (DPC) in a manner analogous to torque and flux control in induction motor, and the controllers are associated with the implementation of sensorless operation. However, the application of such technique to the control of STATCOM and active filters has not been considered so far. In addition, the PWM gating signals are fed directly from the hysteresis controllers in most of the reported papers, fixing the switching frequency of the PWM converter is only discussed in [4][5] based on the motor parameters and is limited to specific motor drive applications.

This paper explains the instantaneous active and reactive power terms based on previous works [12][13][14], and formulates the appropriate power terms for the direct power control of shunt-connected active filters, which are different from those applied in synchronous rectifiers that have been reported so far. In addition, high performance switching functions are derived systematically based on power injection requirement under different compensating conditions. Since the phase information of the PCC voltage is used for the selection of the switching states, this paper also presents a novel algorithm to identify the sectors where the voltage vector is located. The proposed voltage phase tracking algorithm only involves simple algebraic and logical computations, and avoids intensive trigonometric functions as well as consequent approximation errors. Furthermore, the proposed controller adjusts dynamically the bandwidth of the hysteresis comparators and limits the PWM switching frequency to protect the converter in extreme noisy cases.

Compared to the multi-loop control structure, the proposed DPC control directly uses power terms as control variables and integrates control and modulation functions. Therefore, the associated current and voltage control loops, coordinate transformation and separate PWM modulator used in multi-loop control are no longer required in the proposed DPC control. Compared to the DPC control applications in previous works, the proposed method is oriented to improve the performance of active filters, the switching functions are re-defined and the bandwidths of the DPC controllers are dynamically adjusted to limit the averaged switching frequency. The proposed DPC controller is tested on a 2 kVA laboratory prototype for load harmonics filtering and load fluctuation compensation respectively. Simulation and experimental results confirm that the proposed DPC control is robust and insensitive to load conditions, and provides good dynamic and steady state performance.

II. DESCRIPTION OF THE PROPOSED SYSTEM

The shunt-connected active filter uses a standard three-phase two-level voltage source converter, as Fig. 1 shows. For the proposed DPC control scheme, four state variables, the instantaneous active and reactive power of the nonlinear load and those of the active filter, are computed

0-7803-8399-0/04/$20.00 ©2004 IEEE.

continuously. The power terms of the nonlinear load are used to generate the control reference, and those of the active filter are fed back to compare with the control reference. Two hysteresis comparators are used for control purpose and the PWM gating signals are generated based on the output of the comparators. The output of the dc-bus voltage regulation loop is transformed and treated as an instantaneous active power quantity and added to the corresponding control reference. The dynamic separation of the control system is based on the fact that the response of the dc-bus voltage regulation loop is slower than that of the instantaneous power control loop (harmonic and reactive power compensation). The DPC control structure results in averaged waveform synthesis, and the instantaneous power of the system varies within the hysteresis band. During each switching action, a voltage vector is chosen to force the compensator output power following the reference waveform.

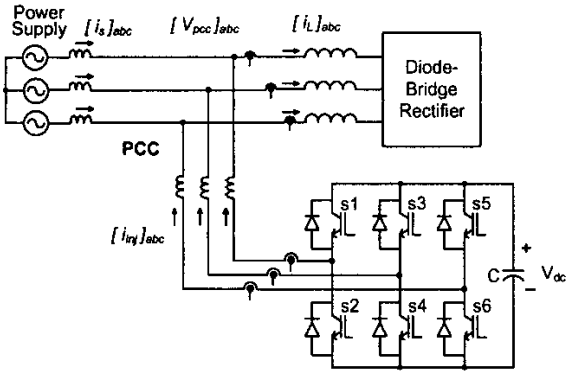

Fig. 1 The power circuit of the shunt-connected active filter.

The entire control algorithm is carried out in the stationary *abc* co-ordinates, without the need of *abc-dq0* transformation. The theory of instantaneous power in three-phase ac system is applied. The instantaneous power terms used in this paper are similar to those of the application reported in [11]. However, in the reported work, the instantaneous power control is implemented through a current control method based on *abc-dq0* transformation. Therefore, forward and backward matrix calculation between the current and the instantaneous power has to be performed. The proposed DPC method directly uses power quantities and results in simple control architecture.

To compensate the fluctuating load current, the commonly used control method is to use the current control approach. It senses and compensates the distorted current to eliminate current harmonics. The dc bus capacitor voltage is regulated through fundamental frequency current injection to charge or discharge the dc bus energy storage capacitor.

The proposed direct power control, comparing with the current control method, is quite different in reference generation and control loop structure. It regulates the converter output voltage amplitude and phase angle according to the power injection requirement and eliminate the intermediate step of regulating the injected current. The dc bus voltage is also regulated based on power requirement in the mean time. In addition, the control and PWM functions are integrated into one loop.

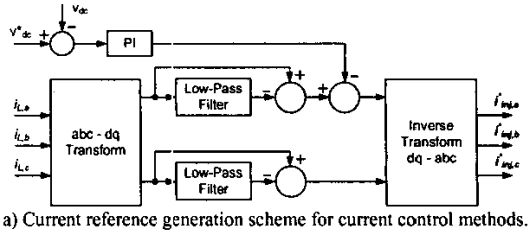

a) Current reference generation scheme for current control methods.

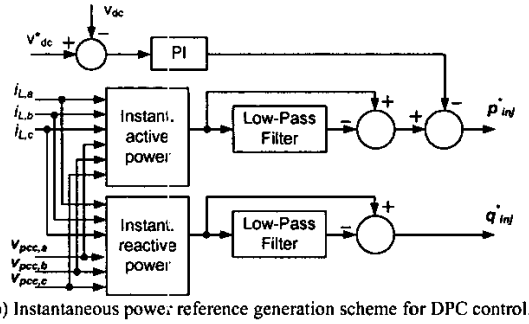

b) Instantaneous power reference generation scheme for DPC control.

Fig. 2 Comparison of different control reference generation schemes.

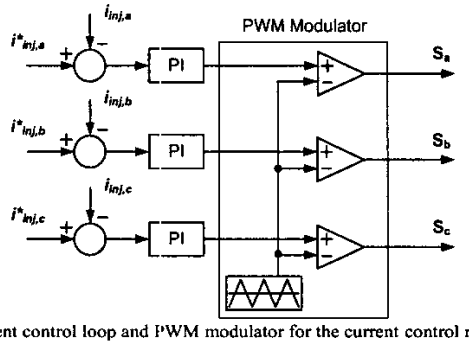

a) Current control loop and PWM modulator for the current control method.

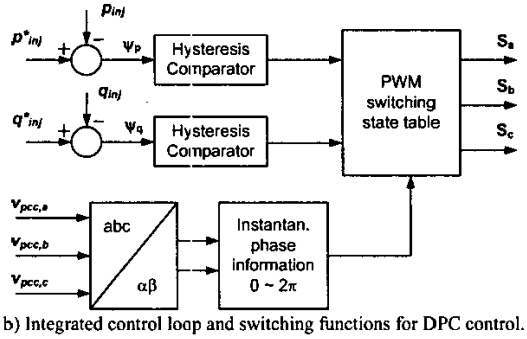

b) Integrated control loop and switching functions for DPC control.

Fig. 3 Comparison of different control structures and PWM methods.

Using simplified block diagrams, the different control reference generation schemes are shown in Fig. 2, and the different control loop structures are illustrated in Fig. 3.

The proposed direct power control compensates the power ripples drawn by the nonlinear load, and forces the instantaneous active power p and reactive power q to be constants on the input side, as the power system is supplying a three-phase balanced linear load.

III. THE SELECTION OF PWM SWITCHING FUNCTIONS

With DPC control scheme, the instantaneous active and reactive power of the active filter are regulated with two hysteresis comparators, and the instantaneous power ripples drawn from the power system are limited within the hysteresis band. This type of control is equivalent to an averaged waveform synthesis.

The simplified equivalent circuit of the active filter and the corresponding vector diagram are illustrated in Fig. 4. During each switching action, one switching vector is selected based on the status of the instantaneous power terms and the sector in which the PCC voltage vector is currently residing.

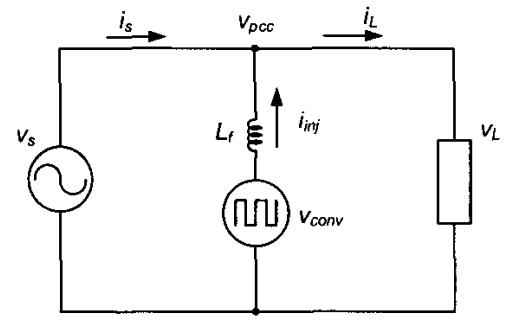

a) Simplified equivalent circuit of the active filter.

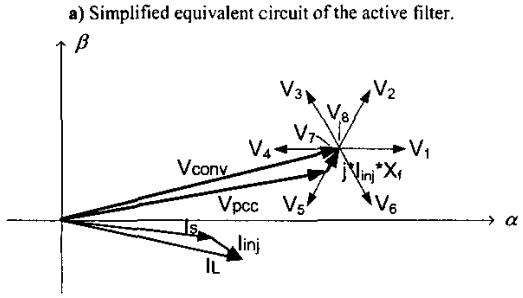

b) Vector diagram illustrating the selection of switching vectors.

Fig. 4 Simplified diagrams of the active filter with DPC control.

A *Sector Division Methods*

One of the straightforward methods divides the α–β plane into six sectors separated by the six voltage space vectors. This kind of division forms an hexagon with six non-zero voltage space vectors ($\mathbf{V_k}$, k= 1, 2, …, 6), there are two zero vectors ($\mathbf{V_7}$, $\mathbf{V_8}$) at the origin of the plane. Using the widely applied space vector modulation for voltage synthesis, the best tracking is obtained when two of the non-zero space vectors adjacent to the reference voltage and one of the zero vectors are selected to synthesize the reference voltage. While in direct power control applications, the control reference is changed to instantaneous power terms from voltage vectors. It is shown that space vector modulation could not be used directly to provide instantaneous power control.

However, this kind of sector division technique can be extended to track the instantaneous power reference with modified switching functions. This is based on the fact that controlling the magnitude and phase angle of the converter output voltage also regulates the output power of the converter at the same time.

Another sector division method is to separate the six sectors to centre with the six voltage space vectors. This kind of division gets the same instantaneous power control performance as the first method.

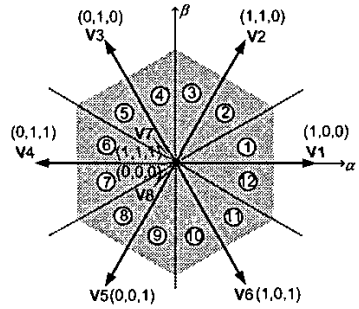

Fig. 5 The twelve-sector division method in α–β plane.

It is shown that a more effective way is to divide the plane into twelve portions, as shown in Fig. 5. It combines the advantage of the two six-sector division methods. Considering the inherent symmetry, the phase angle range of the twelve sectors in the stationary α–β co-ordinates is expressed as

$$(\pi/6)(n-1) < \Theta_n \le (\pi/6)n \qquad n = 1,2,...,12 \qquad (1)$$

The DPC control requires a high sampling frequency of the DSP controller, to minimize the switching time error and prevent the instantaneous injected power of the converter from exceeding the hysteresis boundaries. But experimental results prove that the averaged switching frequency of the converter stays at the same range as that using the conventional current control strategy and standard PWM modulation.

B *Derivation of the Switching State Table*

In direct power control, the instantaneous active power command p^* is generated based on the instantaneous active power ripples drawn by the non-linear load, plus the power requirement of the dc-bus voltage control loop. The instantaneous reactive power command q^* equals to the instantaneous reactive power ripples consumed by the non-linear load. After compensation, the ac system provides only the balanced and averaged power portion of the nonlinear load, and the active filter supplies all of the instantaneous power ripples. If the power rating of the active filter is large enough, it can also inject all of the reactive power required by the load, including both the averaged reactive power component and the reactive power ripples, and unity power factor is achieved at the utility side in this case.

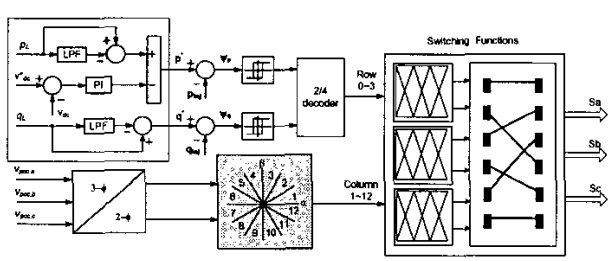

Fig. 6 Block diagram of the proposed direct power control system.

The block diagram of the direct power control system is shown in Fig. 6. The instantaneous power terms of the nonlinear load and those of the active filter are inputs to the hysteresis comparators. After a two-to-four decoder, the comparator output determines the row value of the switching table. The column value is the sector number where the voltage vector exists, and is divided into 12 segments.

By applying an appropriate switching vector to the power converter, the change of the converter instantaneous power can be driven to the desired direction. The voltage space vector can take one out of eight possible positions (including six non-zero vectors and two zero vectors). The influence of each voltage vector ($\mathbf{V_1}$ - $\mathbf{V_8}$) on the change of instantaneous active and reactive power is different, and this leads to different control dynamics.

Table 1 Principles for Switching Vector Selection

Power errors	Criteria for the choose of switching vectors	Application examples (in sector 1)
$\psi_q \geq 0$	Select the voltage vector that makes the converter output voltage lag in phase, as capacitive effect.	Choosing $\mathbf{V_1}$ (1,0,0) or $\mathbf{V_6}$ (1,0,1) in the case of $\psi_p \geq 0$.
		Choosing $\mathbf{V_7}$ (1,1,1), $\mathbf{V_8}$ (0,0,0) or $\mathbf{V_5}$ (0,0,1) in the case of $\psi_p < 0$.
$\psi_q < 0$	Select the voltage vector that makes the converter output voltage lead in phase, as inductive effect.	Choosing $\mathbf{V_2}$ (1,1,0) in the case of $\psi_p \geq 0$.
		Choosing $\mathbf{V_7}$ (1,1,1), $\mathbf{V_8}$ (0,0,0), $\mathbf{V_3}$ (0,1,0) or $\mathbf{V_4}$ (0,1,1) in the case of $\psi_p < 0$.
$\psi_p \geq 0$	Select the voltage vector that makes the converter output voltage increase, acting as a power source.	Choosing $\mathbf{V_1}$ (1,0,0) or $\mathbf{V_6}$ (1,0,1) in the case of $\psi_q \geq 0$.
		Choosing $\mathbf{V_2}$ (1,1,0) in the case of $\psi_q < 0$.
$\psi_p < 0$	Select the voltage vector that makes the inverter output voltage decrease, acting as a load.	Choosing $\mathbf{V_7}$ (1,1,1), $\mathbf{V_8}$ (0,0,0) or $\mathbf{V_5}$ (0,0,1) in the case of $\psi_q \geq 0$.
		Choosing $\mathbf{V_7}$ (1,1,1), $\mathbf{V_8}$ (0,0,0), $\mathbf{V_3}$ (0,1,0) or $\mathbf{V_4}$ (0,1,1) in the case of $\psi_q < 0$.

Table 2 Switching Functions Based on Instantaneous Power Comparison.

Row		Column 1	2	3	4	5	6	7	8	9	10	11	12
0	$\psi_p < 0$ $\psi_q < 0$	0, 1, 0	0, 1, 1	0, 1, 1	0, 0, 1	0, 0, 1	1, 0, 1	1, 0, 1	1, 0, 0	1, 0, 0	1, 1, 0	1, 1, 0	0, 1, 0
1	$\psi_p < 0$ $\psi_q \geq 0$	0, 0, 1	1, 0, 1	1, 0, 1	1, 0, 0	1, 0, 0	1, 1, 0	1, 1, 0	0, 1, 0	0, 1, 0	0, 1, 1	0, 1, 1	0, 0, 1
2	$\psi_p \geq 0$ $\psi_q < 0$	1, 1, 0	1, 1, 0	0, 1, 0	0, 1, 0	0, 1, 1	0, 1, 1	0, 0, 1	0, 0, 1	1, 0, 1	1, 0, 1	1, 0, 0	1, 0, 0
3	$\psi_p \geq 0$ $\psi_q \geq 0$	1, 0, 0	1, 0, 0	1, 1, 0	1, 1, 0	0, 1, 0	0, 1, 0	0, 1, 1	0, 1, 1	0, 0, 1	0, 0, 1	1, 0, 1	1, 0, 1

Assuming the voltage vector is located in sector 1 as illustrated in Fig. 5, the general selection criteria of the converter switching vectors is summarized in Table 1. From which, it can be seen that the instantaneous power control algorithm is quite different from the current control scheme of active filters. Applying the operation principles to the twelve sectors in general cases, a two-dimensional switching state table is derived in Table 2. During implementation, the switching information S_a, S_b and S_c are provided by the look-up table that is stored in the memory of the controller hardware.

IV. CALCULATION OF THE SECTOR NUMBER

Real time implementation of DPC control requires the calculation of the sector number where the PCC voltage vector is currently residing in α–β plane. Usually, the calculation of the sector number requires computing the phase angle θ of the voltage vector at every sampling instant. The computation uses the trigonometric functions, and is usually an approximation by means of interpolation based on a look-up table stored in memory.

This paper proposes a new algorithm to compute the sector number. The algorithm only uses simple algebraic and logical computations, and avoids the calculation of phase angles and the consequent errors. Therefore, it saves the DSP processing time for other important tasks such as switching frequency control.

It can be induced that the two adjacent vectors (V_i and V_{i+1}) of the output voltage vector V_{pcc} correspond to the two largest components among the six values of $|V_k| \cdot |V_{pcc}| \cdot \cos\theta_k$, $k = 1,2,\ldots,6$.

After some mathematical manipulation, it's easy to calculate the numerical values. Taking $k = 2$ as an example,

$$|V_2| \cdot |V_{pcc}| \cdot \cos\theta_2 = \begin{bmatrix} V_{2,\alpha} & V_{2,\beta} \end{bmatrix} \cdot \begin{bmatrix} V_{pcc,\alpha} \\ V_{pcc,\beta} \end{bmatrix} \quad (2)$$
$$= (0.5 \cdot V_{pcc,a} + 0.5 \cdot V_{pcc,b} - V_{pcc,c}) \cdot V_{dc}$$

Applying the same principle to all of the six vectors, the following equations are obtained,

$$\begin{aligned} n_1 &= (V_{pcc,a} - 0.5 \cdot V_{pcc,b} - 0.5 \cdot V_{pcc,c}) \cdot V_{dc} \\ n_2 &= (0.5 \cdot V_{pcc,a} + 0.5 \cdot V_{pcc,b} - V_{pcc,c}) \cdot V_{dc} \\ n_3 &= (-0.5 \cdot V_{pcc,a} + V_{pcc,b} - 0.5 \cdot V_{pcc,c}) \cdot V_{dc} \\ n_4 &= -n_1 \quad n_5 = -n_2 \quad n_6 = -n_3 \end{aligned} \quad (3)$$

It should be noted that the voltage vectors of interest ($V_{pcc,a}$, $V_{pcc,b}$, $V_{pcc,c}$) are the instantaneous PCC bus voltage vectors at the axis *a*, *b* and *c* respectively. In the case of balanced three-phase ac systems, the instantaneous voltage vector can be obtained directly from the sensed three-phase voltages. While in unbalanced and distorted three-phase ac systems, the aforementioned algorithm is not applicable. This limits the applicability of the proposed algorithm to the power systems with good quality voltage supplies, such as applications of active filters or power quality compensators with series device to compensate line voltage and parallel device to compensate line current.

```
IF( j>i )
  {IF (i==1&& j==6) n=12; ELSE n=2i-1;}
ELSE
  {IF(i==6&& j==1) n=11; ELSE n=2i-2;}
```
(4)

Now the problem of computing sector number is transformed into the process of finding the largest element n_i and the second largest element n_j at every sampling time

interval. There are limited possibilities for the values of i and j, and the sector number is determined based on the logic function of (4).

V. CONTROL OF THE PWM SWITCHING FREQUENCY

In practical implementation, the highest switching frequency of the IGBT power devices should be limited to a certain range according to its power rating. A method is investigated in this section by using variable bandwidth of the hysteresis comparators.

Some algorithms have been reported in literature [4][5] for fixing the switching frequency of the PWM converter with hysteresis controllers. The reported algorithm calculates an appropriate hysteresis bandwidth of the current at every sampling instant based on the pre-selected switching time interval. While in direct power control, the control variables are power terms that involve both voltage and current. It is computational intensive to predict a proper hysteresis bandwidth at every sampling instant in order to obtain a constant switching frequency, and the estimation errors may cause the system oscillation. The proposed method is aimed at limiting the averaged switching frequency of the converter and is summarized as following:

i) The setting range of the hysteresis bandwidth and switching frequency is determined based on the observation of the steady state performance of active filters. In the specific experimental prototype used in this paper, the switching frequency varies between 5 kHz to 8 kHz, and the bandwidth range is 2-5 var (0.04 – 0.09 pu). Choosing a switching frequency lower than 5 kHz or using a bandwidth larger than 5 var may introduce severe harmonics.

ii) Small hysteresis bandwidth causes unnecessary high switching frequency in many cases, and large bandwidth introduces high harmonic contents. During the transient states, a large bandwidth is used to limit the switching frequency within 8 kHz. When the system becomes stable, the hysteresis bandwidth is adjusted to a small value to reduce the switching harmonics.

iii) The switching frequency is calculated based on the number of rising edges of the switching pulse in half a cycle (8.3 ms). If the switching frequency is higher than 7.5 kHz (63 pulses), the bandwidth is increased, and when the switching frequency is lower than 6.5 kHz (54 pulses), the bandwidth is decreased.

These design guidelines are implemented with the DSP controller. After design optimization of the proposed control system, the DSP controller has enough processing time for PWM quality improvement. The proposed flowchart for switching frequency control is shown in Fig. 7.

Besides the limitation of the switching frequency, another important issue in PWM implementation is to introduce a certain dead time between the upper and lower IGBT power devices of the three converter legs, to prevent possible short through. The following logic is implemented to control the delay-on of IGBT power switches.

$$y(t_n) = x(t_n) * x(t_{n-1}); \quad (5)$$

For the PWM waveforms as shown in Fig. 8, the computed PWM switching signals in Fig. 8 **a)** is regulated to the waveforms of Fig. 8 **b)** and **c)** respectively for upper and lower power switches on the same converter leg. It is shown that the switch-on command is delayed by a user-defined time interval, which is tunable according to PWM switching frequency. Whereas the switch-off command is executed immediately without any delay

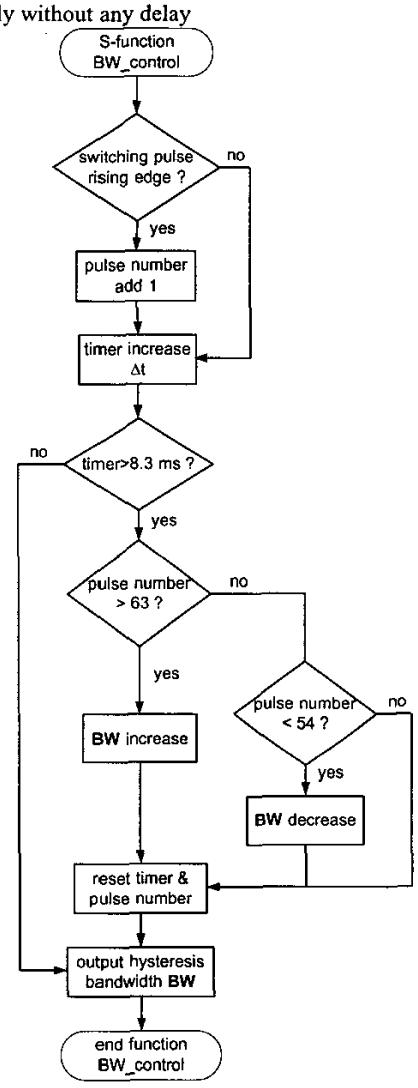

Fig. 7 PWM switching frequency control using variable hysteresis bandwidth.

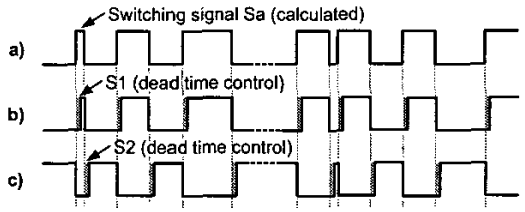

a) Calculated PWM switching commands, b) upper-switch pulses with PWM dead time control, c) lower-switch pulses with dead time control.

Fig. 8 PWM switching dead time control on phase-a.

VI. Simulation and Experimental Results

A laboratory prototype of the active filter is built up based on a 2 kVA converter. The active filter is coupled to the ac system in parallel to handle with unbalanced and nonlinear loads. The power source supplies the averaged power drawn by the load, and consumed by the active filter for compensating switching losses and maintaining a stable dc-bus voltage. The active filter supplies the instantaneous power ripples consumed by the nonlinear load.

The DSP sampling frequency is much higher than the PWM switching frequency in DPC control. For load harmonics compensation, the averaged switching frequency is 7 kHz, while the DSP sampling frequency is 50 kHz in order to filter out the current harmonics and keep the line current sinusoidal. For unbalanced linear load compensation, the averaged switching frequency is 3 kHz, and the DSP sampling frequency is 30-50 kHz in order to track the load power ripples. This is because the DSP has to find the exact moment to switch on or off the converter IGBT power devices. High DSP sampling frequency effectively reduces the switching time errors, and ensures the active filter to inject the exact amount of instantaneous power to the ac systems.

A Harmonic Current Compensation

The experimental results of the active filter are presented in Fig. 9 for filtering the harmonic current caused by a diode-bridge rectifier load. Fig. 9 **a)** shows that the load current is distorted, while the power supply current remains sinusoidal after compensation, and the active filter injects the harmonics drawn by the non-linear load. Fig. 9 **b)** shows the spectrums of the corresponding currents. The main harmonic contents of the load current include 5^{th}, 7^{th}, and 13^{th} components. And the spectrum in bottom indicates that the active filter injects the corresponding harmonic components. Fig. 9 **c)** shows instantaneous power ripples injected by the active filter. The power ripples include multiple frequency components, and the majority of them are 5^{th} and 7^{th} components.

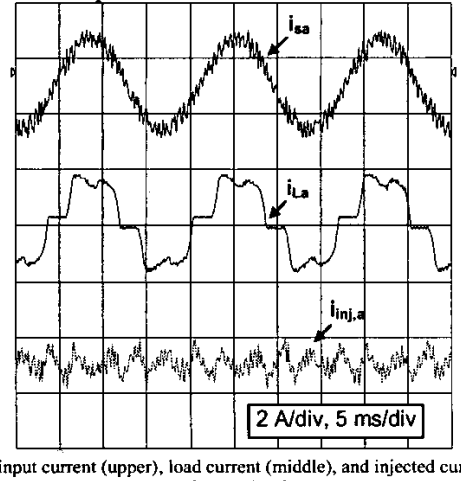

a) The input current (upper), load current (middle), and injected current (lower) of the active filter.

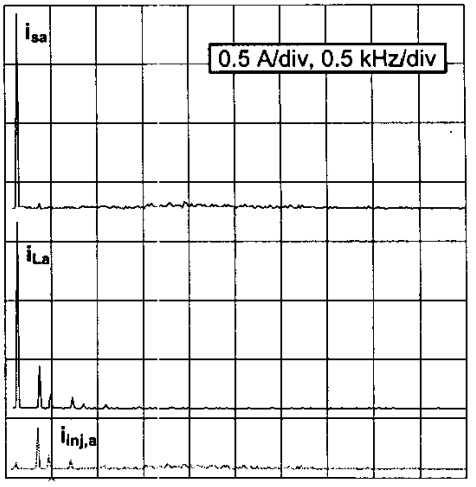

b) Harmonic spectrum of input current (upper), load current (middle) and injected current (lower).

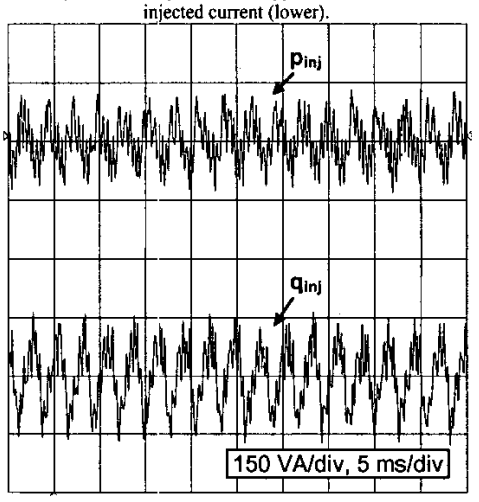

c) Injected instantaneous power p (upper) and q (lower), the ripple is around 300 Hz ~ 420 Hz.

Fig. 9 Performance of the active filter for harmonic current filtering.

B Unbalance Current Compensation

In order to test the dynamic response of the proposed DPC controller, the experiment of the compensator working with three-phase unbalanced load is performed. As initial conditions, the power system is stable and the three-phase load is balanced and linear. Then the load in one phase is suddenly reduced to 50 %, consequently, the total load is unbalanced and reduced. Fig. 10 **a)** shows the three-phase load current is unbalanced and reduced, while the three-phase line current is nearly balanced after compensation. Fig. 10 **b)** shows that the active filter injected instantaneous power is almost zero when the three-phase system is balanced, and a power ripple of 120 Hz is injected when the load is unbalanced. The settling time for line current compensation is around 7 ms.

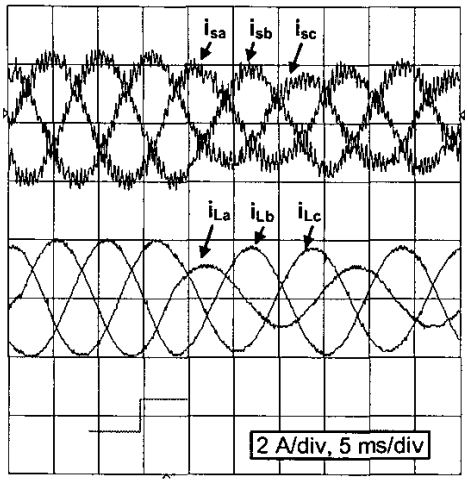

a) The three-phase supply current (upper) and load current (lower) with load in phase-*a* reduced to 50 %. x-axis: 5 m/div, y-axis: 2 A/div.

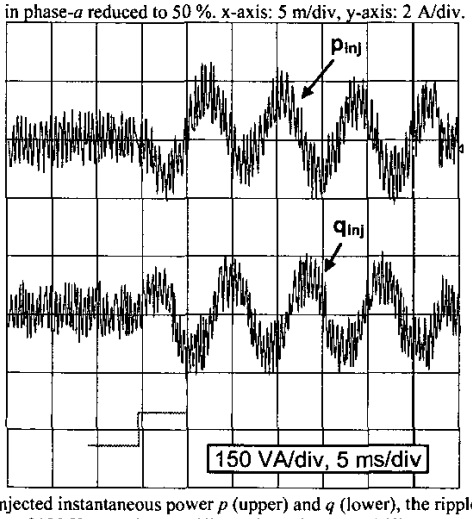

b) The injected instantaneous power *p* (upper) and *q* (lower), the ripple is of 120 Hz, x-axis: 5 ms/div, and y-axis: 150 VA/div.

Fig. 10 Performance of the compensator for unbalanced load compensation.

C *The Averaged Switching Frequencies and PWM Dead-Time Control*

From the PWM patterns and the associated harmonic spectrums as shown in Fig. 11 **a)**, it can be seen that the switching harmonics are distributed in a range from 5.5 – 7 kHz. Therefore, the switching frequency is not fixed, and switching action depends on the output status of the hysteresis comparator. The converter switching frequency would change following the change of the harmonic contents of the load current, as well as the bandwidth of the hysteresis comparator. But the converter switching frequency varies around a certain range when the system is stable. For the specific active filter investigated in this paper, the averaged switching frequency is 7 kHz for nonlinear load compensation, and the averaged switching frequency is 3 kHz for unbalanced linear load compensation.

In Fig. 11 **b)**, a dead-band time is introduced to the PWM gating signals, to prevent short through in the converter legs. Every switch-on action is delayed by 10 μs, to wait the other switch in the same leg to be fully turned off, based on an averaged switching cycle time of 167 μs (switching frequency of 6 kHz) in the experiment. Large dead-band time causes switching harmonics. Therefore, a small and variable dead-band time should be inserted based on the averaged switching frequency.

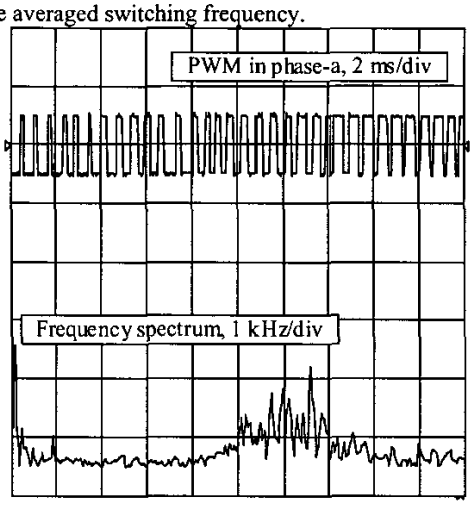

a) PWM switching pulses (upper) and harmonic spectrum (lower). The switching frequency is not fixed, and distributed from 5.5 ~ 7 kHz.

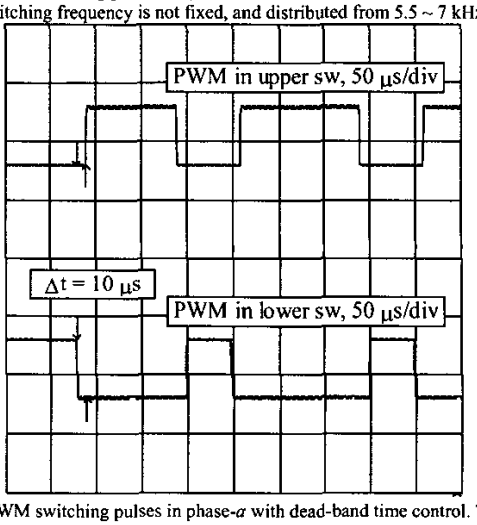

b) PWM switching pulses in phase-*a* with dead-band time control. The switching-on moments are delay by 10 μs with an averaged switching cycle time of 167 μs (switching frequency of 6 kHz).

Fig. 11 Typical PWM switching patterns of the compensator with DPC control.

D *Limiting the Averaged PWM Switching Frequencies*

In order to limit the averaged IGBT switching frequency, the bandwidth of the two hysteresis comparators is regulated according to the measured switching pulse number in each half a cycle time (8.3 ms). Fig. 12 **a)** shows the response of the varying switching frequency by regulating the comparator bandwidth. It is seen that the DSP controller reduces the bandwidth gradually when the switching frequency is less than 7 kHz, as a consequence, the switching frequency increases accordingly. On the other hand, the bandwidth is tuned to increase when the switching

frequency is higher than 8 kHz, so as to force the switching frequency to decrease. The change of the PWM switching frequency always follows the regulation of the bandwidth. Results show that the switching frequency is controlled in the range of 5.5 – 8.5 kHz by using the variable bandwidth between 2 – 5 var. Fig. 12 **b)** lists the averaged switching frequencies in function of the comparator bandwidths for harmonic current compensation. When the bandwidth is larger than 12 var, the converter switching frequency fluctuates. It's hard to define the averaged switching frequency under this condition, and a large amount of harmonics is injected into the power system.

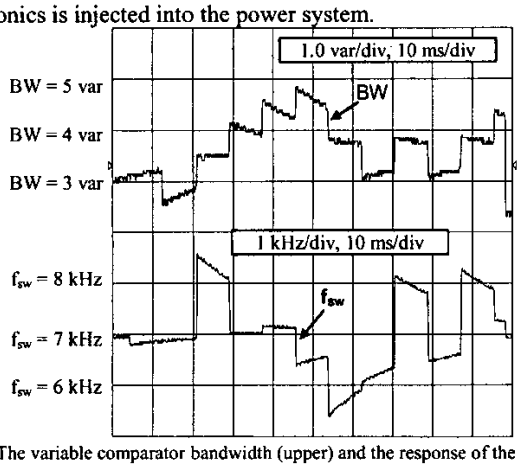

a) The variable comparator bandwidth (upper) and the response of the PWM switching frequency (lower).

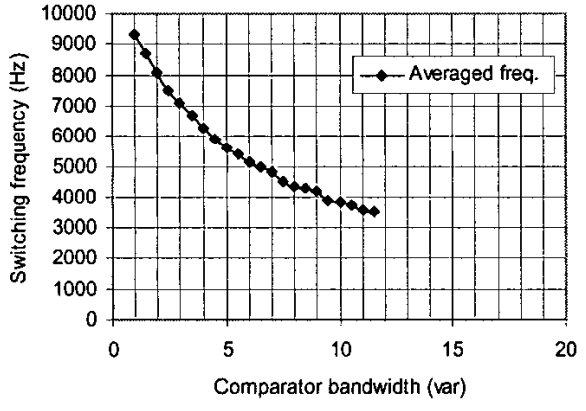

b) The averaged switching frequency in function of the bandwidth of hysteresis comparators.

Fig. 12 Variable bandwidth control to limit the PWM switching frequency.

VII. CONCLUSION

In this paper, a direct power control algorithm (DPC) is proposed and implemented for shunt-connected active filters. The DPC control is extended from the DTC control of motor drives, and significant modifications have been made to the re-definition of the appropriate power terms and the selection of PWM switching functions. With DPC control, the instantaneous active and reactive power terms are directly used as control variables, in addition, the ac current and dc-bus voltage control blocks are integrated into a single control loop. Therefore, the multi-loop control structure is avoided, and the dynamic response is increased. A new algorithm is proposed to get the instantaneous phase information of the PCC voltage vectors that has to be sent to the DPC controller in every sampling time step. The proposed voltage phase tracking method only uses simple algebraic and logical computations, and does not involve any of the trigonometric functions, so it is free of approximation errors and saves DSP controller processing time. Aimed at practical implementation, the limitation of PWM switching frequencies, PWM switching dead-band time control, as well as the high sampling frequency requirement of the DSP controller are considered during the control system design. Simulation and experimental results verify the theoretical analysis.

REFERENCES

[1] T. Noguchi, H. Tomiki, S. Kondo, I. Takahashi, "Direct power control of PWM converter without power source voltage sensors," *Trans. Ind. Appl.*, vol. 34, no.3, pp. 473-479, May/June 1998.

[2] M. Malinowski, M. P. Kazmierkowski, S. Hansen, F. Blaabjerg, and G. D. Marques, "Virtual-flux-based direct power control of three-phase PWM rectifiers," *IEEE Trans. on Industry Applications*, vol. 37, no. 4, pp. 1019-1027, July-Aug. 2001.

[3] G. Escobar, A. M. Stankovic, J. M. Carrasco, E. Galvan, and R. Ortega, "Analysis and design of direct power control (DPC) for a three phase synchronous rectifier via output regulation subspaces," *IEEE Trans. on Power Electronics*, vol.18, no.3, pp.823-830, May 2003.

[4] J. W. Kang, S. K. Sul, "Analysis and prediction of inverter switching frequency in direct torque control of induction machine based on hysteresis bands and machine parameters," *IEEE Trans. on Industry Electronics*, vol. 48, no. 3, pp. 545-553, June 2001.

[5] J. W. Kang, S. K. Sul, "New direct torque control of induction motor for minimum torque ripple and constant switching frequency," *IEEE Trans. on Industry Applications*, vol. 35, no. 5, pp. 1076-1082, Sept./Oct. 1999.

[6] Y. S. Lai, J. C. Lin, "New hybrid fuzzy controller for direct torque control induction motor drives", IEEE Trans. on Power Electronics, vol.18, no.5, pp.1211-1219, Sept. 2003.

[7] J. H. Lee, C. G. Kim, M. J. Youn, "A dead-beat type digital controller for the direct torque control of an induction motor," *IEEE Trans. on Power Electronics*, vol.17, no.5, pp.739-746, Sept. 2002.

[8] E. Monmasson, A. A. Naassani, and J. P. Louis, "Extension of the DTC concept", IEEE Trans. on Industrial Electronics, vol.48, no.3, pp.715-717, June 2001.

[9] R. Datta, and V. T. Ranganathan, "Direct power control of grid-connected wound rotor induction machine without rotor position sensors," *IEEE Trans. on Power Electronics*, vol.16, no.3, pp.390-399, May 2001.

[10] D. Casadei, G. Serra, and A. Tani, "The use of matrix converters in direct torque control of induction machines", IEEE Trans. on Industrial Electronics, vol.48, no.6, pp.1057-1064, Dec. 2001.

[11] V. Soares, P. Verdelho, G. D. Marques, "An instantaneous active and reactive current component method for active filters," *IEEE Trans. on Power Electronics*, vol.15, no.4, pp.660-669, July 2000.

[12] H. Akagi, S. Ogasawara, H. Kim, "The theory of instantaneous power in three-phase four-wire systems: a comprehensive approach," *Conf. Rec. IEEE IAS'99*, Oct. 1999, Phoenix, AR, USA, pp. 287-292.

[13] F. Z. Peng, G. W. Ott, D. J. Adams, "Harmonic and reactive power compensation based on the generalized instantaneous reactive theory for three-phase four-wire systems," *IEEE Trans. Power Elec.*, vol. 13, no. 6, pp. 1174-1181, Nov. 1998.

[14] F. Z. Peng, J. S. Lai, "Generalized instantaneous reactive power for three-phase power systems," *IEEE Trans. Instrum. Meas.*, vol. 45, no. 1, pp. 293-297, Feb. 1996.